Size *vs* Surface: Tuning the Photoluminescence of Freestanding Silicon Nanocrystals Across the Visible Spectrum *via* Surface Groups

Mita Dasog,[†] Glenda B. De los Reyes,[‡] Lyubov V. Titova,[‡,§] Frank A. Hegmann,[‡] and Jonathan G. C. Veinot[†,*]

[†]Department of Chemistry, University of Alberta, Edmonton, Alberta T6G 2G2, Canada, and [‡]Department of Physics, University of Alberta, Edmonton, Alberta T6G 2E1, Canada. [§]Present address: Department of Physics, Worcester Polytechnic Institute, Worcester, MA, 01609, USA.

ABSTRACT The syntheses of colloidal silicon nanocrystals (Si-NCs) with dimensions in the 3−4 nm size regime as well as effective methodologies for their functionalization with alkyl, amine, phosphine, and acetal functional groups are reported. Through rational variation in the surface moieties we demonstrate that the photoluminescence of Si-NCs can be effectively tuned across the entire visible spectral region without changing particle size. The surface-state dependent emission exhibited short-lived excited-states and higher relative photoluminescence quantum yields compared to Si-NCs of equivalent size exhibiting emission originating from the band gap transition. The Si-NCs were exhaustively characterized using transmission electron microscopy (TEM), X-ray photoelectron spectroscopy (XPS), and Fourier transformed infrared spectroscopy (FTIR), and their optical properties were thoroughly investigated using fluorescence spectroscopy, excited-state lifetime measurements, photobleaching experiments, and solvatochromism studies.

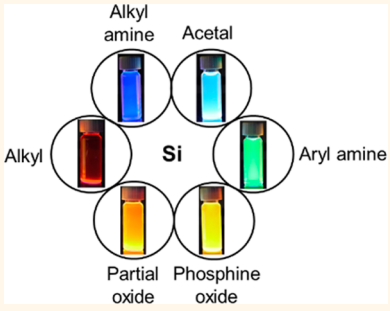

KEYWORDS: silicon nanocrystals · photoluminescence · ligands · surface states · quantum dots · excited-state lifetimes

Silicon is a semiconductor that has always dominated the microelectronics industry.[1−4] For no less than two decades, there has been a concerted effort to develop silicon-based photonics that could exploit existing silicon micro- and nanofabrication technologies to create optical devices. Furthermore, Si-based materials are even more attractive given their biocompatibility[5−7] and its abundance in the Earth's crust.[8] Following the discovery of luminescent porous silicon by Canham,[9] nanostructured Si has held great promise in the development of Si-based light-emitting devices.[10] Today, both porous silicon and freestanding silicon nanocrystals (Si-NCs) have demonstrated proof-of-concept applications in sensors,[11−13] bioimaging,[7,14−16] optical devices,[17−20] photovoltaics,[21−23] water-splitting,[24] batteries,[25,26] among others. Despite the beneficial qualities of Si-NCs, they are still generally viewed as a poor optical material when compared to direct band gap III−V[27−29] and II−VI[30−32] semiconductor quantum dots. Nanocrystalline Si with particle sizes above ∼1.5 nm exhibit an indirect band gap,[33] rendering the emission of light from the material relatively inefficient: a significant amount of energy is often lost *via* nonradiative relaxation processes, and the photoluminescence (PL) quantum yield is dramatically reduced.[9,34−36]

Reports of photoemission from freestanding Si-NCs spanning the entire visible spectrum are scant and have been shown extensively for hydride terminated Si-NCs.[37−39] Unfortunately the hydride surface is prone to oxidation and requires further surface protection. Upon surface functionalization with alkyl groups the PL from Si-NCs often switches to the orange-red visible region.[40,41] The vast majority of reports on Si-NCs emit in the blue visible region irrespective of particle size.[42−46] While such emission has been attributed to oxide defects,[47−50] our group recently demonstrated that this results from an oxynitride species.[51−53] Emissions of this type exhibit short-lived excited-states and often show higher photoluminescent quantum

* Address correspondence to jveinot@ualberta.ca.

Received for review July 24, 2014 and accepted September 2, 2014.

Published online September 02, 2014
10.1021/nn504109a

yields. It is becoming increasingly evident that surface states and interfacial defects play crucial roles in determining the optical properties of Si-NCs.

In recent years, doping of Si-NCs with shallow impurities has been explored as a potential route to enhance the PL properties. Si-NCs have been doped or codoped with phosphorus, boron, and nitrogen atoms.[54−61] While researchers initially observed improvement in PL properties of phosphorus and boron doped Si-NCs, it quickly became evident that the enhancement was sensitive to dopant concentrations, fabrication methods, and location of the dopant atoms. These factors are not easily controlled, hence doping is not a straightforward method to tailor the optical properties of Si-NCs. Surface engineering can offer a means of creating brighter Si-NCs with tunable PL and shorter lifetimes. Recently, Nie *et al.* reported tunable full-color emission in carbon nanoparticles originating from surface states.[62] While such reports of enhancement have appeared, none exist describing a systematic effort to alter the surface groups to tune the PL maxima in Si-NCs.

Herein, we report the syntheses of Si-NCs with an average diameter of 3−4 nm and surfaces passivated with different functional groups. In doing so, we have tuned the PL across the visible spectrum without altering the particle size. The excited-state lifetimes of these emissions are short-lived (nanosecond) and their relative PL quantum yields are higher than those observed for equivalent Si-NCs emitting from a quantum confined state. Photoluminescence excitation (PLE) was also conducted to characterize the excitonic processes/electronic energy levels in the functionalized Si-NCs. The relative stability of the Si-NCs under ambient conditions and under illumination was also investigated.

RESULTS AND DISCUSSION

We demonstrated previously that oxide-embedded Si-NCs are readily obtained *via* disproportionation of commercially available HSQ at high temperature (*ca.* 1100 °C).[39] Hydride terminated Si-NCs are routinely obtained following removal of the oxide matrix upon treatment with an alcoholic HF acid solution. Because hydride terminated Si-NCs are prone to oxidation and not colloidally stable, their surfaces are frequently passivated with alkyl groups by way of various hydrosilylation strategies employing terminal alkenes.

Inert Atmosphere Dodecyl Functionalization of Si-NCs. For the present study dodecyl groups were installed *via* thermally induced hydrosilylation using established literature procedures (Scheme 1).[51]

A representative FTIR spectrum (Figure S1, Supporting Information (SI)) of dodecyl functionalized Si-NCs prepared in inert atmosphere shows characteristic C−H and C−C stretching features at *ca.* 2900 and 1450 cm^{-1}, respectively. There is no evidence of Si−H (*ca.* 2100 cm^{-1}), C═C (*ca.* 1600 cm^{-1}) or Si−O (*ca.* 1100 cm^{-1}) at the sensitivity of FTIR analysis consistent with effective functionalization and negligible oxidation. Figure 1A shows a typical bright field TEM image of oxide free dodecyl functionalized Si-NCs. The average NC diameter is 3.5 ± 0.6 nm. The fit XP spectrum (Figure 1B) shows presence of Si(0), Si(I), and Si(II) with the $2p_{3/2}$ peaks centered at approximately 98.5, 99.8, and 101.0 eV, respectively. The Si(I) and Si(II) contributions have previously been ascribed to surface Si atoms covalently attached to the more electronegative C atoms linking the NC surface to pendant alkyl groups.

Dodecyl functionalized Si-NCs prepared in this way show characteristic red PL centered at *ca.* 730 nm (Figure 1C). The peak intensity of the PL emission

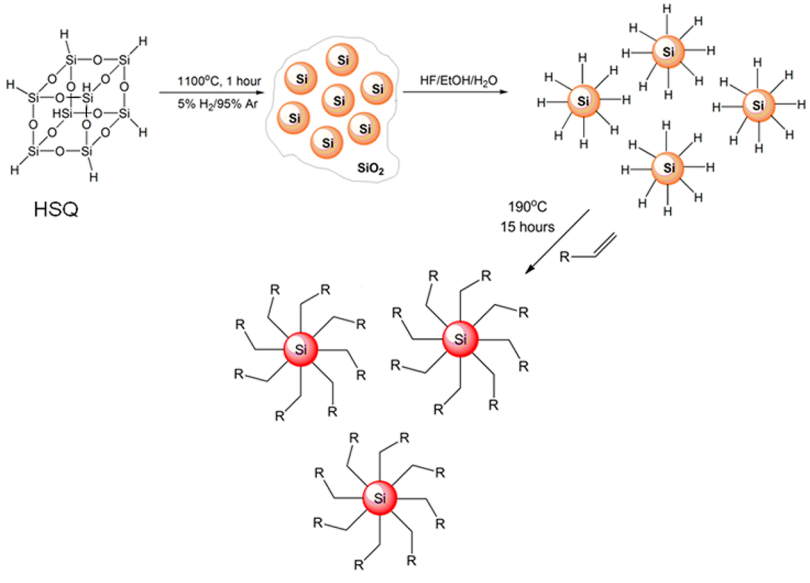

Scheme 1. Schematic representation of synthesis of alkyl functionalized Si-NCs in inert atmosphere.

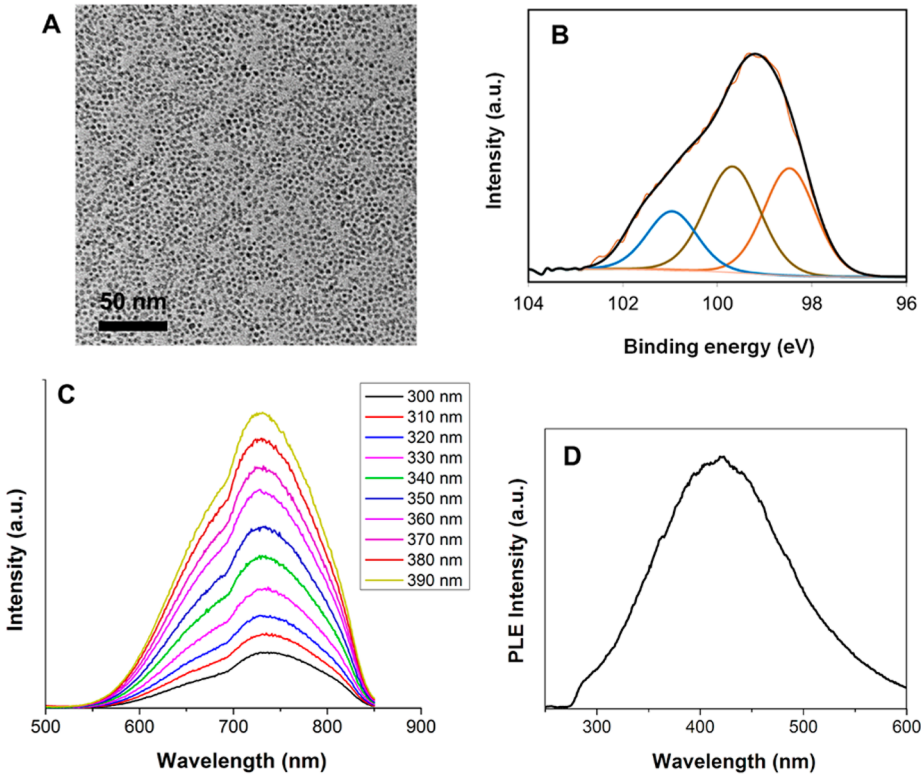

Figure 1. Characterization summary for dodecyl functionalized Si-NCs under inert atmosphere. (A) Bright field TEM image. (B) High resolution XP spectrum of Si 2p region. (Black line corresponds to the fitted peak. For clarity purposes only $2p_{3/2}$ peak fittings are shown.) (C) PL spectra at indicated excitation wavelengths and (D) PLE spectrum at emission maximum (730 nm).

increases with excitation wavelength, there is no detectable shift in the PL maximum. The PLE spectrum (Figure 1D) shows a maximum at *ca.* 420 nm. Previously we determined the excited-state lifetimes of these NCs to be in the microsecond regime (*i.e.*, 19 μs).[51] The optical properties of dodecyl functionalized Si-NCs prepared in inert atmosphere are consistent with the effective mass approximation (EMA);[63] upon the basis of these observations we conclude the PL results from a band gap transition. The colloidal solution of Si-NCs prepared in this way did not photobleach upon continuous excitation at 400 nm for *ca.* 200 min (Figure S2 (SI)), the PL maximum is independent of the solvent polarity, and the relative quantum yield was found to be *ca.* 12%. Thus, prepared alkyl-functionalized Si-NCs are stable under ambient conditions for at least three years, which was concluded by monitoring the PL and FTIR spectrum of the NCs overtime.

Dodecyl Functionalization of Si-NCs in Air. When the hydrosilylation of Si-NCs is performed in air the reaction proceeds readily at 110 °C. Under these conditions, it has been proposed oxygen acts as a radical initiator that facilitates reaction at temperatures lower than 190 °C.[64] In addition to promoting the hydrosilylation reaction, oxygen reacts with Si-NC surfaces leading to partial surface oxidation (Scheme 2) which is apparent in the FTIR spectrum (Figure S3 (SI)) where a Si−O stretch is noted at *ca.* 1100 cm^{-1}. Other features in the IR spectrum include characteristic alkane C−H

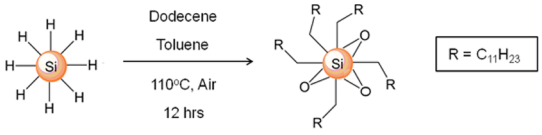

Scheme 2. Schematic representation of alkyl functionalization of Si-NC surface in air.

and C−C stretching at *ca.* 2870 and 1470 cm^{-1}; there is no evidence of alkene absorptions (*i.e.*, ═C—H at ∼ 3050 cm^{-1} and C═C at ∼1600 cm^{-1}) following functionalization. Complete reaction of all silicon hydride surface groups with either dodecene or oxygen is consistent with the absence of Si−H stretch at *ca.* 2100 cm^{-1}. Bright field TEM analysis of these partially oxidized Si-NCs yielded an average diameter of 3.6 ± 0.7 nm (Figure 2A). Oxidation of the Si surface is further confirmed using XPS analysis (Figure 2B). The high resolution Si 2p spectrum shows emissions at 100.1, 101.0, and 101.8 eV corresponding to Si(I), Si(II), and Si(III) oxidation states, respectively. The presence of Si(0) is confirmed by the presence of an emission at 99.2 eV.

The PL spectrum obtained from a toluene solution of partially oxidized Si-NCs showed a maximum emission significantly blue-shifted from that of equivalent dodecyl Si-NCs surface functionalized under inert atmosphere (*vide supra*) centered at *ca.* 630 nm (Figure 2C). A shoulder is observed at *ca.* 710 nm. Similar to the red-emitting dodecyl Si-NCs, only the

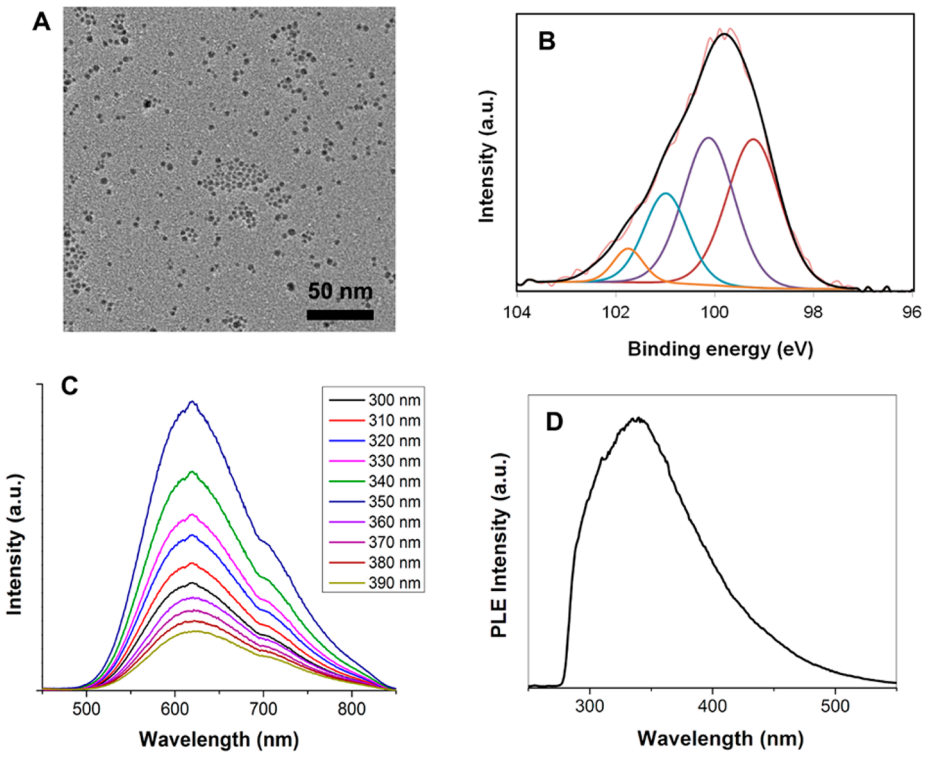

Figure 2. Characterization summary for dodecyl functionalized Si-NCs (functionalization performed in air). (A) Bright field TEM image. (B) High resolution XP spectrum of Si 2p region. (Black line corresponds to the fit spectrum. For clarity only $2p_{3/2}$ peak fittings are shown.) (C) PL spectra at indicated excitation wavelengths and (D) PLE spectrum at emission maximum (630 nm).

intensity of the luminescence changed with excitation wavelength. The PLE spectrum showed a single broad asymmetric absorption peak centered at 340 nm (Figure 2D). PL excited-state lifetime measurements afforded short-lived excited-states with $\tau_1 = 0.4$ ns and $\tau_2 = 2.9$ ns (Figure S4 (SI)) at 650 nm; however, no microsecond component was observed. The short-lived excited-state and blue-shifted PL have previously been attributed to a Si═O moiety based upon computational models;[65] however, to our knowledge no molecular equivalent of this functional group exists without substantial stabilization. In this context, and that no conclusive evidence can be obtained from the presented methods, it is not possible to confidently confirm presence of Si═O. While the origin of this emission (*e.g.*, band gap or surface mediated transition) is difficult to conclusively identify; however, in light of the excited-state lifetime it likely results from a hereforeto unidentified surface state. The present oxide/alkyl surface modified Si-NCs solution showed no detectable photobleaching upon continued excitation at 340 nm for 250 min (Figure S5 (SI)) and were found to be stable over one year under ambient conditions (determined using PL and FTIR spectroscopy). The relative photoluminescent quantum yield was found to be 18%, and the PL maximum was independent of the solvent polarity.

Surface Modification of Si-NCs upon Reaction with Trioctylphosphine Oxide. Molecular silanes reduce phosphine oxides to their parent trisubstituted phosphine.[66,67] It is reasonable similar reactivity will be observed for hydride terminated Si-NCs. In this vein, hydride terminated Si-NCs were reacted with trioctylphosphine oxide (TOPO). Under the presented conditions, hydride surface moieties on the Si-NCs are expected to reduce TOPO to trioctylphosphine (TOP); because the reaction is carried out in air any TOP produced by the reaction is oxidized back to TOPO (Scheme 3). The particles are subsequently stabilized by TOPO and rendered soluble in organic solvents. Of important note, upon reaction of hydride terminated Si-NCs with TOPO under inert conditions TOP is formed (confirmed using ^{31}P NMR, Figure S6 (SI)). TOP does not coordinate to the Si-NC surface and the oxidized particles are insoluble in organic solvents.

Unfortunately, following reaction with TOPO it is not possible to conclusively identify the exact identity of the oxidized Si-NC surface. It is reasonable upon the basis of XPS and FTIR data that it consists of bridging Si−O−Si moieties. Figure S7 (SI) shows the FTIR spectra of neat TOPO and TOPO Si-NCs. In both spectra, P═O stretching at *ca.* 1120 cm^{-1}, C−H stretches *ca.* 2870, 1470, and 1370 cm^{-1} are observed. A weak Si−O stretch is observed in TOPO Si-NC sample at 1080−1040 cm^{-1} consistent with the presence of oxide. The oxidation of the particles is more obvious in the features XPS analysis. The high resolution XP spectrum of Si 2p region shows Si(I) and Si(II) peaks

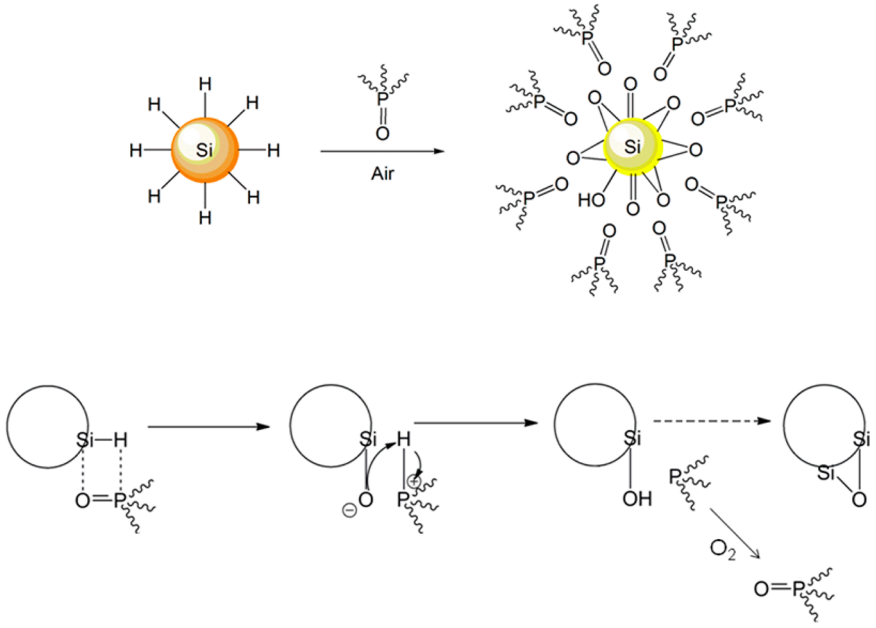

Scheme 3. Schematic representation of reactivity of Si hydride surface with TOPO.

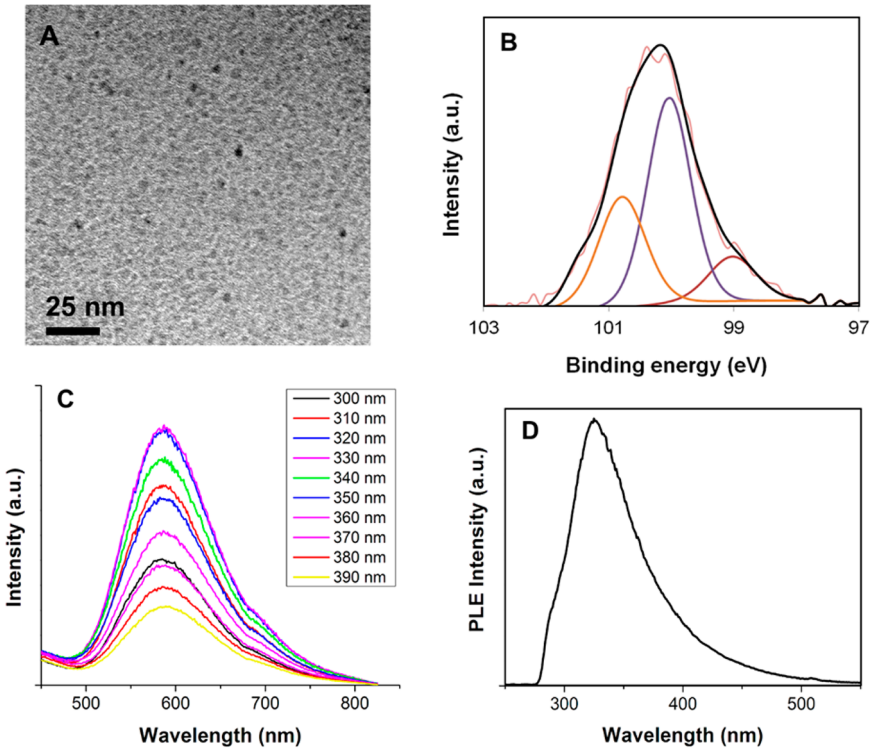

Figure 3. Characterization details for TOPO Si-NCs. (A) Bright field TEM image. (B) High resolution XP spectrum of Si 2p region. (Black line corresponds to the fit data. For clarity only $2p_{3/2}$ peak fittings are shown.) (C) PL spectra at indicated excitation wavelengths and (D) PLE spectrum at emission maximum (590 nm).

ca. 100 and 100.8 eV, respectively (Figure 3B). The Si(0) peak is at 99 eV confirms the particles are not completely oxidized.

Bright field TEM imaging shows Si-NCs with an average diameter of 3.2 ± 0.5 nm; however, the quality of the image is poor due to the presence of large excess of organic ligand (Figure 3A). Attempts to remove the excess TOPO *via* selective precipitation and low temperature crystallization resulted in agglomeration/precipitation of the Si-NCs.

TOPO surface modified Si-NCs show a PL maximum at 590 nm (Figure 3C) that exhibits excitation wavelength dependent intensity. The PLE spectrum shows maximum centered at 315 nm when measured at the

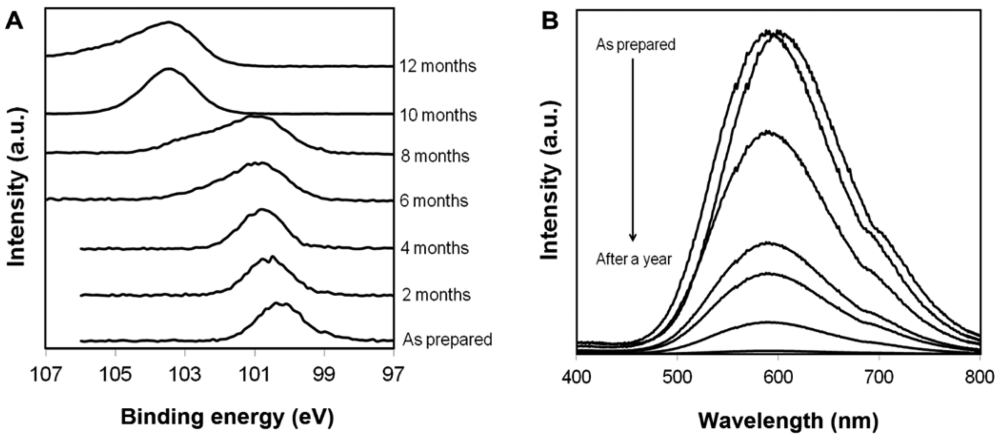

Figure 4. (A) High resolution XP spectra of Si 2p region for TOPO Si-NCs at various intervals over a year. (B) Evolution of the PL spectra of TOPO Si-NCs over one year. Spectra were collected for a freshly prepared sample and then after 2, 4, 6, 8, 10, and 12 months.

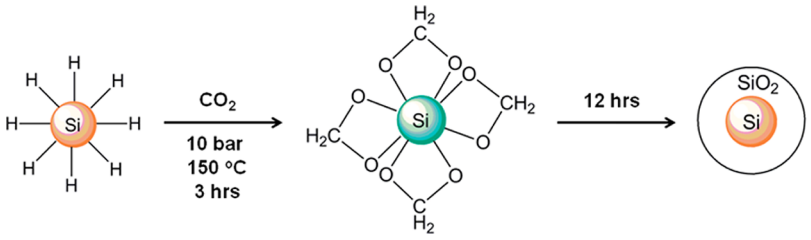

Scheme 4. Reaction of hydride terminated Si-NCs with CO_2.

emission maximum (Figure 3D). The excited-state lifetime analysis confirmed presence of both microsecond and nanosecond components (Figure S8 (SI)). As was the case for the orange-emitting dodecyl functionalized Si-NCs (*vide supra*), it is reasonable the nanosecond lifetime originates from an oxide-based defect state and the microsecond lifetime from the band gap. Upon continuous excitation at 315 nm for 250 min, the TOPO stabilized Si-NCs solution show decreased photoluminescence intensity (Figure S9 (SI)). The relative quantum yield was determined to be 17% and the PL maximum was independent of the solvent polarity. Of particular importance to the present discussion, we found the oxidation of TOPO Si-NCs continues and proceeds slowly over a year. XPS analysis shows an increase in Si oxidation state as the Si 2p peak shifts toward higher binding energies with prolonged aging time (Figure 4A) and no signal was observed for Si(0) after 8 months. Initially a moderate blue-shift of the PL maximum is observed, followed by complete PL quenching (Figure 4B).

CO_2 Reaction with Si-NCs. To further explore the reactivity of hydride terminated Si-NCs, toluene solutions of particles were exposed to high pressure (10 bar)/temperature (150 °C) CO_2 for 3 h. Spectroscopic analysis indicates the resulting Si-NCs were surface terminated with acetal groups as shown pictorially in Scheme 4. Longer reaction times (*i.e.*, > 12 h) yielded formaldehyde and oxide coated Si-NCs. Previously, CO_2 has been converted to methanol upon reaction with silane reducing agents; however, these homogeneous molecular reactions were catalyzed using carbenes or ammonia-borane complexes at room temperature.[68,69] In the present study, CO_2 reduction proceeds without an external catalyst; however, a minimum temperature of 150 °C and 10 bar pressure are required. Figure S10 (SI) shows key spectral regions within the FTIR spectrum of Si-NCs as the reaction with CO_2 proceeds. The Si−H stretches *ca.* 2100 and 920 cm^{-1} are dominant features in freshly prepared hydride terminated Si-NCs. After 3 h, C−H stretch *ca.* 2920 cm^{-1} and C−O, Si−O−C, Si−O−Si stretches between 1300−1080 cm^{-1} appear. After 12 h the Si-NCs precipitate from the reaction mixture due to complete surface oxidation and the IR of this solid shows spectral features corresponding to Si−O−Si stretching at *ca.* 1100 cm^{-1}. A weak C−H stretch is also observed at 2900 cm^{-1}. The acetal stabilized Si-NCs have an average diameter of 3.4 ± 0.5 nm as determined from TEM analysis (Figure 5A). The high resolution XP spectrum of Si 2p region for acetal Si-NCs show, Si(0), Si(I), Si (II), and Si(IV) oxidation states with peaks at 98.8, 100.3, 101.4, and 103.5 eV, respectively (Figure 5B).

The present acetal terminated Si-NCs photoluminesce in the blue-green spectral region and exhibit excitation wavelength dependent PL maximum (Figure 5C). It is reasonable this excitation wavelength dependence arises from multiple surface states consistent

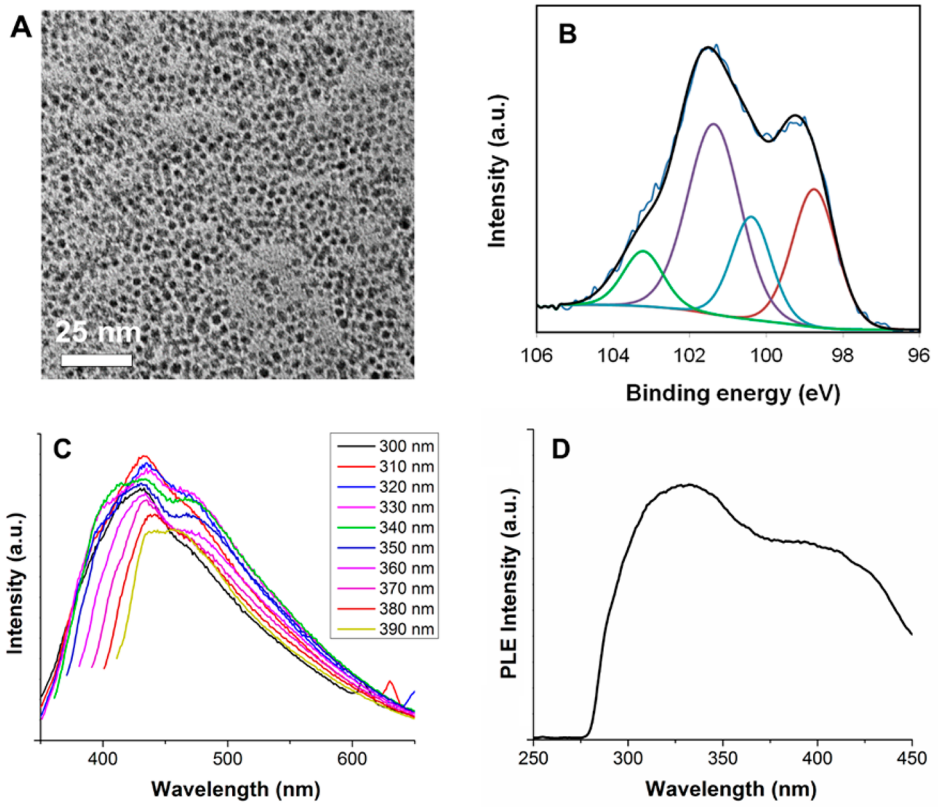

Figure 5. Characterization details for acetal functionalized Si-NCs. (A) Bright field TEM image. (B) High resolution XP spectrum of Si 2p region. (Black line corresponds to fit data. For clarity only $2p_{3/2}$ peak fittings are shown.) (C) PL spectra at indicated excitation wavelengths and (D) PLE spectrum at emission maximum (470 nm).

with the presence of different maxima in the PLE spectrum (Figure 5D). Similar luminescence has been observed in carboxylic acid functionalized Si surfaces[70,71] and oxidized silicon carbide (SiC) NCs.[72,73] Upon the basis of literature reports, we tentatively attribute the blue-green PL to a charge transfer state involving a silicon carboxy site. To further confirm this phenomenon, solvatochromic studies were performed and the PL showed red-shift with increasing solvent polarity consistent with a charge transfer process (Figure S11 (SI)). Excited-state lifetime analysis at 485 nm showed short-lived states, with $\tau_1 = 1.4$ and $\tau_2 = 5.4$ ns (Figure S12 (SI)). The relative quantum yield was 22%. The acetal functionalized Si-NCs solution showed significant photobleaching upon exposure to constant illumination of 300 nm light (Figure S13 (SI)); however, they were found to be stable under ambient conditions for extended period of time (>6 months).

N-Bonded Dodecylamine Functionalized Si-NCs. Reaction of hydride terminated Si-NCs with PCl_5 affords chloride terminated Si particles.[53] These particles offer a convenient platform with which to react alkyl amines. Because PCl_5 etches Si surfaces,[74] d−5 nm hydride terminated Si-NCs were used for this reaction to allow direct comparison with hydrosilylated and TOPO modified Si-NCs (*vide supra*). No effort was made to isolate the chloride terminated particles; following removal of excess PCl_5 particles were reacted directly with dodecylamine under mild heating (*i.e.*, 40 °C) as summarized in Scheme 5.

The FTIR spectra of neat dodecylamine and dodecylamine modified Si-NCs are shown in Figure S14 (SI). Characteristic N−H stretches (*ca.* 3300−3100 and 1600 cm^{-1}) are observed in neat dodecylamine but are absent from the Si-NC spectrum consistent with amine group reacting with silicon surface. Absorptions attributable to C−H stretches from the alkyl chain are observed at *ca.* 2900 and 1470 cm^{-1} in neat dodecylamine and functionalized Si-NCs. Partial oxidation of Si-NCs is evidenced by Si−O−Si stretch features *ca.* 1120 cm^{-1}. The high resolution XP spectrum of Si 2p region shows two distinctive peaks corresponding to Si(0) core atoms with peak at 98.8 eV and surface Si atoms attached to either N or O with peak at 102 eV (Figure 6A). The N 1s region can be fit to two peaks. The peak at 397.8 eV is characteristic of bridging nitrogen atoms (Si−N−Si). The species responsible for the emission at 399.5 eV remains unclear; however, we tentatively assigned to silicon oxynitride type of species (Figure 6B).[51]

TEM analysis indicates the present dodecylamine functionalized Si-NCs possess an average particle size for 3.8 ± 0.7 nm (Figure 6C). The dodecylamine Si-NCs photoluminesce in the blue spectral region (Figure 6D)

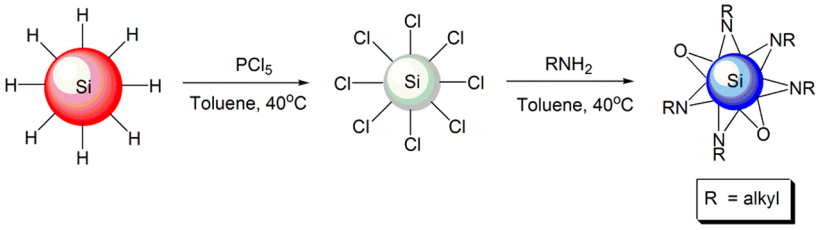

Scheme 5. Schematic representation of synthesis of dodecylamine functionalized Si-NCs.

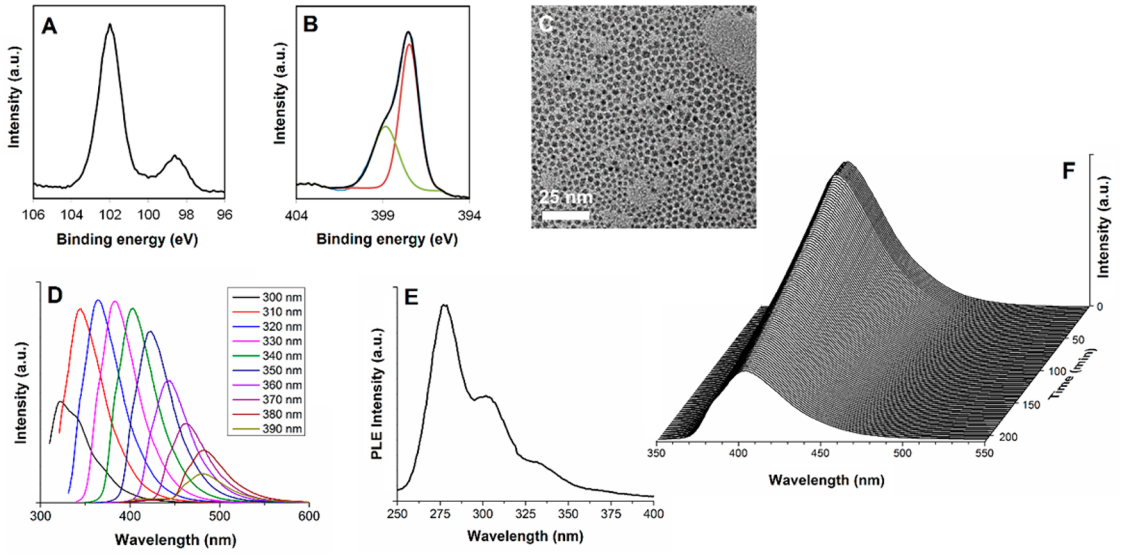

Figure 6. Characterization details for dodecylamine functionalized Si-NCs. High resolution XP spectra of (A) Si 2p region and (B) N 1s region. (Black line corresponds to the fit data.) (C) Bright field TEM image, (D) PL spectra at indicated excitation wavelengths, (E) PLE spectrum with emission at 410 nm, and (F) emission overtime under continuous illumination (λ_{ex} = 300 nm).

and the excited-state lifetimes showed fast decay with τ_1 = 1.5 ns and τ_2 = 6.5 ns (Figure S15 (SI)) measured at 470 nm. These NCs also show excitation wavelength dependence and multiple local maxima in the PLE spectrum (Figure 6E). Previously, we have proposed the blue PL results from a charge transfer state involving silicon oxynitride type species and solvatochromic studies further confirm the presence of charge transfer state (Figure S16 (SI)).[51] The relative quantum yield for these NCs was 32%. Like other Si-NCs presented here, blue-emitting Si-NCs solution photobleaches upon constant excitation at 300 nm; however, the emission was never completely lost (Figure 6F). Thus, functionalized Si-NCs are stable for few months (3−4) but succumb to oxidation over time and precipitate out of the solution.

N-Bonded Diphenylamine Functionalized Si-NCs. Recently, Li *et al.* reported green luminescent diphenylamine functionalized Si-NCs *via* reduction of $SiCl_4$ followed by modification with diphenylamine.[75] The authors reported oxygen is crucial to the appearance of green PL with nanosecond (5 ns) lifetimes. A similar reaction was explored for the chloride terminated Si-NCs obtained from PCl_5 reaction. Again, the chlorination of Si surface was performed by reacting 5−6 nm hydride Si-NCs with PCl_5 followed by reaction with diphenylamine (Scheme 6).

The FTIR spectra of neat diphenylamine and diphenylamine functionalized Si-NCs are shown in Figure S17 (SI). The N−H stretch *ca.* 3400 cm^{-1} disappears after functionalization. The aromatic C−H stretches are observed at *ca.* 3050 and 1000−700 cm^{-1} and C═C stretches at *ca.* 1600−1400 cm^{-1} in both spectra. A weak broad feature is observed at *ca.* 1040 cm^{-1} that is confidently assigned to Si−O−Si stretching. The high resolution XP spectrum of Si 2p region shows two peaks corresponding to Si(0) core at 98.9 eV and surface Si attached to N and O atoms with a peak centered at 101.4 eV (Figure 7A). The N 1s region (Figure 7B) can be fit to three components corresponding to Si−N−Si (398 eV), Si−N−O (399.6 eV), and free diphenylamine (400.8 eV). The average Si-NC size was found to be 3.9 ± 0.5 nm (Figure 7C) from TEM analysis.

The PL maximum of diphenylamine functionalized Si-NCs appears in the green at 512 nm (Figure 7D), red-shifted compared to the emission from alkyl-amine stabilized Si-NCs. Solvatochromic studies showed that the PL maximum is dependent upon solvent polarity (Figure S18 (SI)). As was the case for Li *et al.*, oxidation was crucial for the appearance of green PL. Without surface oxide (which was achieved by longer reaction time, *i.e.*, 48 h), the PL was quenched. Higher degrees of oxidation characteristic of short reaction times (*i.e.*, 6 h)

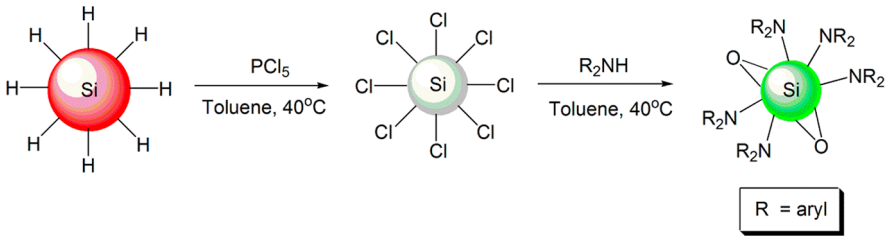

Scheme 6. Schematic representation of synthesis of diphenylamine functionalized Si-NCs.

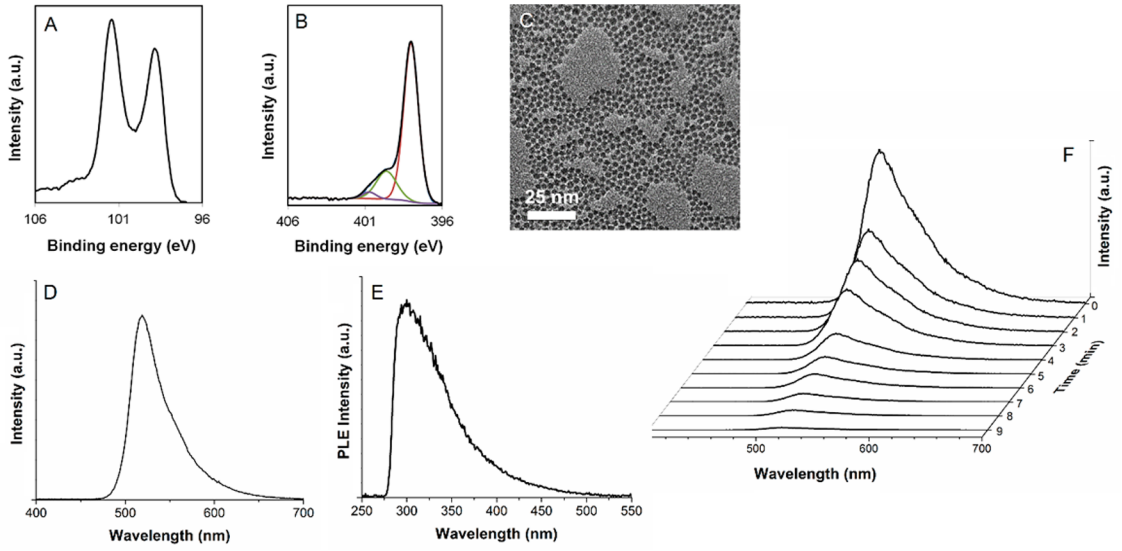

Figure 7. Characterization details for diphenylamine functionalized Si-NCs. High resolution XP spectra of (A) Si 2p region and (B) N 1s region. (Black line corresponds to the fit data.) (C) Bright field TEM image, (D) PL spectrum (λ_{ex} = 350 nm), (E) PLE spectrum with emission maximum (510 nm), and (F) emission overtime under continuous illumination (λ_{ex} = 350 nm).

afforded NCs that were not colloidally stable; further analysis of these materials was not performed. PLE spectrum of the green-emitting Si-NCs obtained after 12 h of reaction with diphenylamine shows a maximum at 305 nm (Figure 7E). Evaluation of excitation wavelength dependent PL shift was precluded by rapid photobleaching (Figure 7F). Unfortunately, solutions of diphenylamine Si-NCs did not exhibit long-term colloidal stability and precipitated from solution after approximately 1 week.

All the Si-NCs prepared for this study had an average particle diameter between 3–4 nm. The widely accepted effective mass approximation (EMA) predicts particles of this size should emit in the spectral region between 670 and 810 nm if the emission arises from a band gap transition. This is consistent with our recent STS investigation of individual Si-NCs.[52] Furthermore, upon the basis of the indirect band gap of bulk Si, it is also reasonable these particles will exhibit microsecond excited-state lifetimes. Clearly this is not the case here: only dodecyl Si-NCs functionalized under inert conditions show the predicted PL properties. Si-NCs that possess oxide-based defect states (*i.e.*, TOPO Si-NCs and dodecyl Si-NCs functionalized in air) show nanosecond and/or microsecond excited-state lifetimes and the PL maximum

Figure 8. Photograph of 3–4 nm Si-NCs functionalized with various surface groups dispersed in toluene, under UV illumination. From left to right the Si-NC functionalization: blue, dodecylamine; blue-green, acetal; green, diphenylamine; yellow, TOPO; orange, dodecyl (air); red, dodecyl (inert).

is blue-shifted compared to EMA predictions. The PL maximum of these Si-NCs does not change with excitation wavelength or the solvent polarity. The emission from these samples likely originates from a composite of surface state and band gap processes.

Alternatively, Si-NCs functionalized with alkyl and aryl amines as well as acetal groups exhibit excitation wavelength dependent photoluminescent with a maximum that red-shifts with increasing solvent polarity. The origin of PL from these functionalized particles can be tentatively attributed to surface group mediated charge transfer processes based upon the nanosecond

excited-state lifetimes and solvatochromic studies. These materials are subject to significant photobleaching upon prolonged excitation. Figure 8 shows the photograph of 3−4 nm Si-NCs with various surface groups under UV-illuminations.

CONCLUSIONS

In conclusion, this is the first report of Si-NC emission where the PL maximum has been tuned across the visible spectrum *via* surface engineering without changing the NC size. We have shown new reactivity of hydride terminated Si-NCs with TOPO and CO_2. Surface state emission allows for fast radiative recombination rates and high relative PL quantum yields. While the specific nature of various emissive sites remains unknown, this study highlights the importance of surface states and the crucial role they play in the optical properties of Si-NCs.

EXPERIMENTAL SECTION

Materials. Hydrogen silsesquioxane (HSQ) was purchased from Dow Corning Corporation (Midland, MI) as FOx-17. 1-Dodecene (97%, Sigma-Aldrich), trioctylphosphine oxide (TOPO, 97%, Sigma-Aldrich), phosphorus pentachloride (PCl_5, 98%, Sigma-Aldrich), dodecylamine (98%, Sigma-Aldrich), diphenylamine (99%, Sigma-Aldrich), hydrofluoric acid (HF, 49%, J. T. Baker), toluene (ACS grade, BDH), anhydrous toluene (Sigma-Aldrich), methanol (MeOH, ACS grade, Sigma-Aldrich), and ethanol (EtOH, ACS grade, Sigma-Aldrich) were used without further purification.

Syntheses of Oxide Embedded Si-NCs. Procedures developed in the Veinot Laboratory that afford well-characterized materials were employed to prepare oxide-embedded silicon nanocrystals (Si-NC/SiO_2). Briefly, solid HSQ (*ca.* 3 g) was placed in a quartz boat and transferred to a Lindberg Blue tube furnace and heated from ambient to a peak processing temperature of 1100 °C at 18 °C min^{-1} in a slightly reducing atmosphere (*i.e.*, 5% H_2/95% Ar). The sample was maintained at the peak processing temperature for 1 h. Upon cooling to room temperature, the resulting amber solid was ground into a fine brown powder using an agate mortar and pestle. This yields oxide embedded Si-NCs with an average diameter of *ca.* 3 nm (Composite **1**). To obtain larger particles, 1.0 g of **1** was transferred to a high temperature furnace (Sentro Tech Corp.) for further thermal processing under argon atmosphere. The composite was heated to 1200 °C at 10 °C/min and maintained at that temparature for an hour and cooled to room temperature. This yielded Composite **2** consisting of Si-NC exhibiting average diameters of *ca.* 6 nm embedded in silica matrix.

Preparation of Hydride Terminated Si-NCs. Freestanding hydride terminated Si-NCs were liberated from their oxide matrix *via* hydrofluoric acid etching. Approximately 0.30 g of Si-NC/SiO_2 composite was transferred to a polyethylene terephthalate beaker and 3 mL of deionized water, EtOH, and 49% HF acid were added with stirring in subdued light. (Caution: Hydrofluoric acid can be extremely dangerous and must be handled with great care.) The resulting dark brown, cloudy mixture was stirred for 1 h. Hydrophobic hydride terminated Si-NCs were extracted from the aqueous etching mixture using three 20 mL toluene extractions. All remaining HF was neutralized using an excess of aqueous saturated solution of calcium chloride. The cloudy dark brown Si-NC/toluene extracts were placed into glass test tubes and centrifuged using a low speed (7000 rpm) centrifuge for 5 min. After centrifugation, the toluene supernatant was decanted leaving a precipitate of hydride terminated Si-NCs.

Synthesis of Dodecyl Functionalized Si-NCs under Inert Atmosphere. Hydride terminated Si-NCs (obtained from **1**) were redispersed in 50 mL of 1-dodecene, and transferred to an oven-dried Schlenk flask. The cloudy brown suspension was degassed using three freeze/pump/thaw cycles and maintained under a dry argon atmosphere. The flask was placed in a silicone oil bath and heated in subdued light to 190 °C for 15 h. Following the reaction, a transparent orange-brown solution was obtained consistent with effective surface modification. The product mixture was divided equally among four 50 mL PTFE centrifuge tubes. NCs were precipitated using a 3:1 mixture of EtOH:MeOH (20 mL). Particles were centrifuged at 14000 rpm for 20 min using a Beckman J2−21 high-speed centrifuge and the supernatant was decanted. Three subsequent dissolution/precipitation/centrifugation cycles were performed using a toluene/MeOH/EtOH mixture (1:3:1). After the final precipitation cycle, the dodecyl functionalized Si-NCs were dispersed in dry toluene, filtered through a hydrophobic PTFE filter, and stored in a glass vial until further use.

Synthesis of Dodecyl Functionalized Si-NCs in Air. Hydride terminated Si-NCs (obtained from **1**) were redispersed in 5 mL of 1-dodecene and 25 mL of toluene. The reaction mixture was refluxed in air and subdued light at 110 °C for 12 h. After reaction, a transparent orange-brown solution was obtained consistent with effective surface functionalization. The reaction mixture was divided equally between four 50 mL PTFE centrifuge tubes. Functionalized NCs were precipitated using a 3:1 mixture of EtOH:MeOH (20 mL). Particles were centrifuged at 14000 rpm for 20 min using a Beckman J2−21 high-speed centrifuge, followed by decanting of the supernatant. Three dissolution/precipitation/centrifugation cycles were performed using a toluene/MeOH/EtOH mixture (1:3:1). After the final precipitation the functionalized Si NCs were dispersed in toluene, filtered through a hydrophobic PTFE filter, and stored in a glass vial until further use.

Synthesis of Trioctylphosphine Oxide (TOPO) Surface Terminated Si-NCs. Hydride terminated Si-NCs (obtained from **1**) were redispersed in 50 mL of toluene containing 2.0 g of TOPO. The reaction mixture was stirred for 8 h under ambient conditions. A clear orange solution was obtained and the NCs were stored in a glass vial until further use. Attempts to remove excess TOPO ligand led to precipitation of the surface oxidized Si-NCs. Therefore, we conclude TOPO is required for stabilization and dissolution of the oxidized Si-NCs in organic solvents.

Reaction of Carbon Dioxide (CO_2) with Si-NCs. Hydride terminated Si-NCs (obtained from **1**) were dispersed in 10 mL dry toluene and transferred to a 100 mL Bergoh high pressure steel reactor maintained under Ar atmosphere. The reaction flask was evacuated and filled with 10 bar CO_2. This was followed by heating at 150 °C for 3 h. The reaction flask was cooled to room temperature and the pressure was released. The reaction mixture consisted of yellow solution containing soluble particles and an orange precipitate. The precipitate was removed *via* centrifugation at 8000 rpm. The supernatant was collected and filtered through a hydrophobic PTFE filter, and stored in a glass vial until further use.

Synthesis of Dodecylamine Functionalized Si-NCs. Hydride terminated Si-NCs (obtained from **2**) were dispersed in 5 mL anhydrous toluene and transferred to a Schlenk flask containing 15 mL dry toluene. 0.35 g of PCl_5 was added to the hydride Si-NCs and stirred together for an hour at 40 °C under Ar atmosphere. Toluene and byproducts including PCl_3 were removed *in vacuo* leaving an orange precipitate. Dry toluene (15 mL) was added to the reaction flask, followed by 0.25 g of dodecylamine. The reaction mixture was heated at 40 °C for 8 h under an Ar atmosphere. The flask was cooled to room temperature and the clear light yellow solution was transferred to a separatory funnel and washed with distilled water thrice to remove excess dodecylamine and hydrochloride salt. The toluene layer was filtered through a hydrophobic PTFE filter, and the particles were stored in a glass vial until further use.

Synthesis of Diphenylamine Functionalized Si-NCs. Hydride terminated Si-NCs (obtained from **2**) were dispersed in 5 mL dry toluene and transferred to a Schlenk flask charged with 15 mL anhydrous toluene. 0.35 g of PCl_5 were added to the hydride terminated Si-NCs and the mixture was stirred for 1 h at 40 °C under an Ar atmosphere. Toluene and byproducts including PCl_3 were removed *in vacuo* leaving an orange precipitate. Dry toluene (15 mL) was added to the reaction flask, followed by 0.30 g of diphenylamine. The reaction mixture was heated at 40 °C for 12 h under Ar atmosphere. The flask was cooled to room temperature and the clear light brown solution was transferred to a separatory funnel and washed with distilled water thrice to remove the hydrochloride salt. Excess diphenylamine was removed *via* crystallization at −20 °C and the crystals were removed by vacuum filtration. The particles were filtered through a hydrophobic PTFE filter, and stored in a glass vial until further use.

Characterization. Fourier transformation infrared spectroscopy (FTIR) was performed using a Nicolet Magna 750 IR spectrometer. Samples were drop coated onto a Si wafer from the respective solutions. Phosphorus nuclear magnetic resonance spectra (^{31}P NMR) were collected using a 500 MHz Varian Inova instrument. UV−vis absorbance spectra were recorded on Cary 400 UV−vis spectrometer.

Transmission electron microscopy (TEM) images were obtained using a Hitachi-9500 electron microscope with an accelerating voltage of 300 (low magnification) and 400 kV (high resolution). TEM samples were prepared by drop coating the Si-NC suspension onto a carbon coated copper grid with a 400 μm diameter hole. The NC size was averaged over 200 particles determined using ImageJ software (version 1.45). The HRTEM images were processed using Gatan DigitalMicrograph software (version 2.02.800.0).

Photoluminescence (PL) and photoluminescence excitation (PLE) spectra of the solution phase samples were acquired using a Varian Cary Eclipse fluorescence spectrometer. Nanosecond (ns) lifetime measurements were performed using an excitation pulse of a 400 nm second harmonic signal from a BBO crystal pumped by 800 nm pulses from a Ti:sapphire laser (Coherent RegA900 with 65 fs pulse width and 250 kHz repetition rate) with average excitation power of 1.88 mW. Time-resolved PL was recorded using a time-correlated single-photon-counting (TCSPC) unit (Picoharp 300, Picoquant) equipped with a single-photon avalanche photodiode (SPAD, PDM Series by Micro Photon Devices) and coupled to a monochromator (Acton SP2500, Princeton Instruments). The TCSPC system has a time resolution of 54 ± 1 ps. A 435 nm long pass filter (Edmund optics) was placed at the entrance of the spectrometer to block scattered laser pulses. For microsecond carrier recombination lifetime measurements, 1 kHz frequency-doubled 400 nm pulses from another Ti:sapphire laser (Coherent Legend Elite, 45 fs pulse width) were used to excite the PL at an average excitation power of 4.5 mW. A fast silicon photodiode (Thorlabs, PDA36A, rise time 20.6 ns) coupled to a 300 MHz oscilloscope (Tektronix) was used to measure the microsecond carrier recombination lifetime. The photodiode was placed at a path perpendicular to the excitation beam and 10 nm bandpass filters (Edmund Optics) were used to select a particular emission wavelength. The carrier recombination lifetimes were accurately fitted by double exponential decay:

$$y(t) = Ae^{-t/\tau_1} + Be^{-t/\tau_2} \quad (1)$$

where τ_1 and τ_2 are the decay times and A and B are the respective amplitudes of the decay components.

XPS analyses were performed using a Kratos Axis Ultra instrument operating in energy spectrum mode at 210 W. The base pressure and operating chamber pressure were maintained at 10^{-7} Pa. A monochromatic Al Kα source (λ = 8.34 Å) was used to irradiate samples, and spectra were obtained with an electron takeoff angle of 90°. To minimize sample charging the charge neutralizer filament was used as appropriate. Survey spectra were collected using an elliptical spot with major and minor axis lengths of 2 and 1 mm, respectively, and 160 eV pass energy with a step of 0.33 eV. CasaXPS software (VAMAS) was used to interpret high-resolution (HR) XP spectra. All spectra were internally calibrated to the C 1s emission (284.8 eV). After calibration, the background was subtracted using a Shirley-type background to remove most of the extrinsic loss structure. The full width at half-maximum (fwhm) for all the fitted peaks was maintained below 1.2 eV.

Photoluminescence Quantum Yield Measurements. Photoluminescence quantum yields were determined using methods adapted from the work of Williams *et al.*[76] 9,10-biphenylanthracene in cyclohexane, Coumarin 1 in absolute ethanol, fluorescein in methanol, rhodamine B in ethanol, and rhodamine 6G in methanol were used as reference dyes. Si-NCs were dissolved in toluene. All organic solvents were passed through a column of anhydrous magnesium sulfate to remove trace moisture prior to preparing the solutions. Stock solutions were prepared by dissolving 10 mg of organic dye in the appropriate solvent with stirring until the solid was completely dissolved. Solutions were filtered through a 200 μm PTFE membrane filter to remove suspended impurities and a series of diluted solution were made with absorbances ranging from 0.1 and 0.01. PL spectra were acquired for the identical solutions and the slit width was maintained from 5−10 depending on the species. The slopes of plots of the integrated fluorescence intensity *versus* UV−vis absorbance curves were determined and compared to ensure the highest quality reference curves. In all cases, experimentally determined photoluminescence quantum yields of the organic dyes were in good agreement with literature values. Slopes of plots of the integrated PL intensity *versus* absorbance were determined for all Si-NC samples and the quantum yields were calculated using the following equation:

$$\phi_x = \phi_{st}\left(\frac{m_x}{m_{st}}\right)\left(\frac{\eta_x^2}{\eta_{st}^2}\right) \quad (2)$$

where ϕ is the photoluminescence quantum yield, m is the slope of the integrated PL intensity *vs* absorbance curve, and η is the refractive index of the solvent. The subscript st refers to the standard organic dye, and x indicates the unknown species being evaluated. The excitation wavelength, slit widths and reference for Si-NC evaluations are listed in the Supporting Information in Table S1.

Conflict of Interest: The authors declare no competing financial interest.

Acknowledgment. The authors acknowledge funding from the National Engineering Research Council of Canada (NSERC), Canada Foundation for Innovation (CFI), Alberta Science and Research Investment Program (ASRIP), Alberta Innovates Technology Futures (AITF), and *iCi*Nano (iCORE Centre for Interdisciplinary Nanoscience). G.D.R. would like thank AITF for support. We would like to thank W. C. Moffat and B. Mason for assistance with FTIR spectroscopy, and G. Popowich and D. Mullin for the technical support the time-resolved PL. The staff at the Alberta Centre for Surface Engineering and Sciences (ACSES) is thanked for XPS analysis. K. Cui at the National Institute of Nanotechnology (NINT) is thanked for TEM analysis. R. Snitynsky is thanked for assistance with NMR. The Veinot group is thanked for useful discussion.

Supporting Information Available: Quantum yield measurement details, FTIR, excited-state lifetimes, solvatochromism studies, and photobleaching data for various functionalized Si-NCs. This material is available free of charge *via* the Internet at http://pubs.acs.org.

REFERENCES AND NOTES

1. Ball, P. Silicon Still Supreme. *Nat. Mater.* **2005**, *4*, 119.
2. Cava, R. J. Solid-State Physics—Super Silicon. *Nature* **2006**, *444*, 427–428.
3. Yates, J. T., Jr. A New Opportunity in Silicon-Based Microelectronics. *Science* **1998**, *279*, 335–336.
4. Kern, D. P.; Kuech, T. F.; Oprysko, M. M.; Wagner, A.; Eastman, D. E. Future Beam-Controlled Processing Technologies for Microelectronics. *Science* **1988**, *241*, 936–944.

5. Liu, J. W.; Erogbogbo, F.; Yong, K. T.; Ye, L.; Liu, J.; Hu, R.; Chen, H. Y.; Hu, Y. Z.; Yang, Y.; Yang, J. H.; *et al.* Assessing Clinical Prospects of Silicon Quantum Dots: Studies in Mice and Monkeys. *ACS Nano* **2013**, *7*, 7303–7310.
6. Bhattacharjee, S.; Rietjens, I. M. C. M.; Singh, M. P.; Atkins, T. M.; Purkait, T. K.; Xu, Z.; Regli, S.; Shukaliak, A.; Clark, R. J.; Mitchell, B. S.; *et al.* Cytotoxicity of Surface-Functionalized Silicon and Germanium Nanoparticles: The Dominant Role of Surface Charges. *Nanoscale* **2013**, *5*, 4870–4883.
7. Erogbogbo, F.; Yong, K.-T.; Roy, I.; Xu, G.; Prasad, P. N.; Swihart, M. T. Biocompatible Luminescent Silicon Quantum Dots for Imaging of Cancer Cells. *ACS Nano* **2008**, *2*, 873–878.
8. Michl, J. Silicon Chemistry. *Chem. Rev.* **1995**, *95*, 1135.
9. Cullis, A. G.; Canham, L. T. Visible Light Emission Due to Quantum Size Effects in Highly Porous Crystalline Silicon. *Nature* **1991**, *353*, 335–338.
10. Pavesi, L.; Turan, R. *Silicon Nanocrystals: Fundamentals, Synthesis and Applications*; Wiley-VCH: Weinheim, 2010.
11. Gonzalez, C. M.; Iqbal, M.; Dasog, M.; Piercey, D. G.; Lockwood, R.; Klapötke, T. M.; Veinot, J. G. C. Detection of High-Energy Compounds Using Photoluminescent Silicon Nanocrystal Paper Based Sensors. *Nanoscale* **2014**, *6*, 2608–2612.
12. Lockwood, R.; Veinot, J. G. C.; Meldrum, A. Sensing Water and Alcohol Vapors with Freestanding Silicon Quantum Dots. *Sens. Lett.* **2013**, *11*, 1535–1540.
13. Yi, Y.; Zhu, G.; Liu, C.; Huang, Y.; Zhang, Y.; Li, H.; Zhao, J.; Yao, S. A Label-Free Silicon Quantum Dots-Based Photoluminescence Sensor for Ultrasensitive Detection of Pesticides. *Anal. Chem.* **2013**, *85*, 1146–11470.
14. Zhong, Y.; Peng, F.; Bao, F.; Wang, S.; Ji, X.; Yang, L.; Su, Y.; Lee, S.-T.; He, Y. Large-Scale Aqueous Synthesis of Fluorescent and Biocompatible Silicon Nanoparticles and Their Use as Highly Photostable Biological Probes. *J. Am. Chem. Soc.* **2013**, *135*, 8350–8356.
15. Nishimura, H.; Ritchie, K.; Kasai, R. S.; Goto, M.; Morone, N.; Sugimura, H.; Tanaka, K.; Sase, I.; Yoshimura, A.; Nakano, Y.; *et al.* Biocompatible Fluorescent Silicon Nanocrystals for Single-Molecule and Fluorescence Imaging. *J. Cell Biol.* **2013**, *202*, 967–983.
16. Borsella, E.; D'Amato, R.; Falconieri, M.; Trave, E.; Panarii, A.; Rivolta, I. An Outlook on the Potential of Si Nanocrystals as Luminescent Probes for Bioimaging. *J. Mater. Res.* **2013**, *28*, 193–204.
17. Hirschman, K. D.; Tsybeskov, L.; Duttagupta, S. P.; Fauchet, P. M. Silicon-Based Visible Light-Emitting Devices Integrated into Microelectronic Circuits. *Nature* **1996**, *384*, 338–341.
18. Pavesi, L.; Dal Negro, L.; Mazzoleni, C.; Franzò, G.; Priolo, F. Optical Gain in Silicon Nanocrystals. *Nature* **2000**, *408*, 440–444.
19. Maier-Flaig, F.; Rinck, J.; Stephan, M.; Bocksrocker, T.; Bruns, M.; Kübel, C.; Powell, A. K.; Ozin, G. A.; Lemmer, U. Multicolor Silicon Light-Emitting Diodes (SiLEDs). *Nano Lett.* **2013**, *13*, 475–480.
20. Cheng, K. Y.; Anthony, R.; Kortshagen, U. R.; Holmes, R. J. Hybrid Silicon Nanocrystal-Organic Light-Emitting Devices for Infrared Electroluminescence. *Nano Lett.* **2010**, *10*, 1154–1157.
21. Liu, C. Y.; Holman, Z. C.; Kortshagen, U. R. Hybrid Solar Cells from P3HT and Silicon Nanocrystals. *Nano Lett.* **2009**, *9*, 449–452.
22. Niesar, S.; Fabian, W.; Petermann, N.; Herrmann, D.; Riedle, E.; Wiggers, H.; Brandt, M. S.; Stutzmann, M. Efficiency Enhancement in Hybrid P3HT/Silicon Nanocrystal Solar Cells. *Green* **2011**, *1*, 339–350.
23. Conibeer, G.; Green, M.; Corkish, R.; Cho, Y.; Cho, E. C.; Jiang, C. W.; Fangsuwannarak, T.; Pink, E.; Huang, Y.; Puzzer, T.; *et al.* Silicon Nanostructures for Third Generation Photovoltaic Solar Cells. *Thin Solid Films* **2006**, *511*, 654–662.
24. Erogbogbo, F.; Lin, T.; Tucciarone, P. M.; LaJoie, K. M.; Lai, L.; Patki, G. D.; Prasad, P. N.; Swihart, M. T. On-Demand Hydrogen Generation Using Nanosilicon: Splitting Water Without Light, Heat or Electricity. *Nano Lett.* **2013**, *13*, 451–456.
25. Graetz, J.; Ahn, C. C.; Yazami, R.; Fultz, B. Highly Reversible Lithium Storage in Nanostructured Silicon. *Electrochem. Solid-State Lett.* **2003**, *6*, A194–A197.
26. Kim, H.; Seo, M.; Park, M.-H.; Cho, J. A Critical Size of Silicon Nano-Anodes for Lithium Rechargeable Batteries. *Angew. Chem., Int. Ed.* **2010**, *49*, 2146–2149.
27. Ashmore, A. D.; Finley, J. J.; Oulton, R.; Fry, P. W.; Lemaitre, A.; Mowbray, D. J.; Skolnick, M. S.; Hopkinson, M.; Buckle, P. D.; Maksym, P. A. Optical Properties of Single Charge Tuneable InGaAs Quantum Dots. *Phys. E* **2002**, *13*, 127–130.
28. Harris, D. K.; Bawendi, M. G. Improved Precursor Chemistry for the Synthesis of III-V Quantum Dots. *J. Am. Chem. Soc.* **2012**, *134*, 20211–20213.
29. Mi, Z.; Chang, Y.-L. III-V Compound Semiconductor Nanostructures on Silicon: Epitaxial Growth, Properties, and Applications in Light Emitting Diodes and Lasers. *J. Nanophotonics* **2009**, *3*, 031602.
30. Dabbousi, B. O.; Rodriguez-Viejo, J.; Mikulec, F. V.; Heine, J. R.; Mattoussi, H.; Ober, R.; Jensen, K. F.; Bawendi, M. G. CdSe)ZnS Core-Shell Quantum Dots: Synthesis and Optical and Structural Characterization of a Size Series of Highly Luminescent Materials. *J. Phys. Chem. B* **1997**, *101*, 9463–9475.
31. Alivisatos, A. P. Semiconductor Clusters, Nanocrystals, and Quantum Dots. *Science* **1996**, *271*, 933–937.
32. Mashford, B. S.; Stevenson, M.; Popovic, Z.; Hamilton, C.; Zhou, Z.; Breen, C.; Steckel, J.; Bulovic, V.; Bawendi, M.; Coe-Sullivan, S.; *et al.* High-Efficiency Quantum-Dot Light-Emitting Devices with Enhanced Charge Injection. *Nat. Photonics* **2013**, *7*, 407–412.
33. Kocevski, V.; Eriksson, O.; Rusz, J. Transition Between Direct and Indirect Band Gap in Silicon Nanocrystals. *Phys. Rev. B: Condens. Matter Mater. Phys.* **2013**, *87*, 245401.
34. Garcia, C.; Garrido, B.; Pellegrino, P.; Ferre, R.; Moreno, J. A.; Pavesi, L.; Cazzanelli, M.; Morante, J. R. Absorption Cross-Section and Lifetimes as a Function of Size in Si Nanocrystals Embedded in SiO_2. *Phys. E* **2003**, *16*, 429–433.
35. Canham, L. T. Gaining Light from Silicon. *Nature* **2000**, *408*, 411–412.
36. Sham, T. K.; Jiang, D. T.; Coulthard, I.; Lorimer, J. W.; Feng, X. H.; Tan, K. H.; Frigo, S. P.; Rosenberg, R. A.; Houghton, D. C.; Bryskiewicz, B. Origin of Luminescence from Porous Silicon Deduced by Synchrotron-Light-Induced Optical Luminescence. *Nature* **1993**, *363*, 331–334.
37. Li, X.; He, Y.; Talukdar, S. S.; Swihart, M. T. Photoluminescent Silicon Nanoparticles with Emission Spanning the Visible Spectrum. *Langmuir* **2003**, *19*, 8490–8496.
38. Pi, X. D.; Liptak, R. W.; Nowak, J. D.; Wells, N.; Blank, D. A.; Carter, C. B.; Campbell, S. A.; Kortshagen, U. Air-Stable Full-Visible-Spectrum Emission from Silicon Nanocrystal Ensembles Synthesized by an All-Gas-Phase Plasma Approach. *Nanotechnology* **2008**, *19*, 123102.
39. Hessel, C. M.; Henderson, E. J.; Veinot, J. G. C. Hydrogen Silsesquioxane: A Molecular Precursor for Nanocrystalline Si-SiO_2 Composites and Freestanding Hydride Surface Terminated Silicon Nanoparticles. *Chem. Mater.* **2006**, *18*, 6139–6146.
40. Gupta, A.; Swihart, M. T.; Wiggers, H. Luminescent Colloidal Dispersion of Silicon Quantum Dots from Microwave Plasma Synthesis: Exploring the Photoluminescence Behavior across the Visible Spectrum. *Adv. Funct. Mater.* **2009**, *19*, 696–703.
41. Gupta, A.; Schulz, C.; Wiggers, H. Influence of Etching and Surface Functionalization on the Optical Property of Luminescing Phosphorus Doped Silicon Nanoparticles. *J. Optoelectron. Adv. Mater.* **2010**, *12*, 518–522.
42. Shiohara, A.; Hanada, S.; Prabakar, S.; Fujioka, K.; Lim, T. H.; Yamamoto, K.; Northcote, P. T.; Tilley, R. D. Chemical Reactions on Surface Molecules Attached to Silicon Quantum Dots. *J. Am. Chem. Soc.* **2010**, *132*, 248–253.
43. Zou, J.; Baldwin, R. K.; Pettigrew, K. A.; Kauzlarich, S. M. Solution Synthesis of Ultrastable Luminescent Siloxane-Coated Silicon Nanoparticles. *Nano Lett.* **2004**, *4*, 1181–1186.

44. Pettigrew, K. A.; Liu, Q.; Power, P. P.; Kauzlarich, S. M. Solution Synthesis of Alkyl- and Alkyl/Alkoxy-Capped Silicon Nanoparticles *via* Oxidation of Mg_2Si. *Chem. Mater.* **2003**, *15*, 4005–4011.
45. Sankaran, R. M.; Holunga, D.; Flagan, R. C.; Giapis, K. P. Synthesis of Blue Luminescent Si Nanoparticles using Atmospheric-Pressure Microdischarges. *Nano Lett.* **2005**, *5*, 537–541.
46. Svrcek, V.; Sasaki, T.; Shimizu, Y.; Koshizaki, N. Blue Luminescent Silicon Nanocrystals prepared by ns Pulsed Laser Ablation in Water. *Appl. Phys. Lett.* **2006**, *89*, 213113–213115.
47. Dohnalova, K.; Zidek, K.; Ondic, L.; Kusova, K.; Cibulka, O.; Pelant, I. Optical Gain at the F-Band of Oxidized Silicon Nanocrystals. *J. Phys. D: Appl. Phys.* **2009**, *42*, 135102.
48. Lioudakis, E.; Othonos, A.; Nassiopoulou, A. G. Ultrafast Transient Photoinduced Absorption in Silicon Nanocrystals: Coupling of Oxygen-Related States to Quantized Sublevels. *Appl. Phys. Lett.* **2007**, *90*, 171103.
49. Luppi, M.; Ossicini, S. *Ab Initio* Study on Oxidized Silicon Clusters and Silicon Nanocrystals Embedded in SiO_2: Beyond the Quantum Confinement Effect. *Phys. Rev. B: Condens. Matter Mater. Phys.* **2005**, *71*, 035340.
50. Brewer, A.; von Haeften, K. *In Situ* Passivation and Blue Luminescence of Silicon Clusters Using a Cluster Beam/H_2O Codeposition Production Method. *Appl. Phys. Lett.* **2009**, *94*, 261102.
51. Dasog, M.; Yang, Z.; Regli, S.; Atkins, T. M.; Faramus, A.; Singh, M. P.; Muthuswamy, E.; Kauzlarich, S. M.; Tilley, R. D.; Veinot, J. G. C. Chemical Insight Into the Origin of Red and Blue Photoluminescence Arising from Freestanding Silicon Nanocrystals. *ACS Nano* **2013**, *7*, 2676–2685.
52. Wolf, O.; Dasog, M.; Yang, Z.; Balberg, I.; Veinot, J. G. C.; Millo, O. Doping and Quantum Confinement Effects in Single Si Nanocrystals Observed by Scanning Tunneling Spectroscopy. *Nano Lett.* **2013**, *13*, 2516–2521.
53. Dasog, M.; Veinot, J. G. C. Size Independent Blue Luminescence in Nitrogen Passivated Silicon Nanocrystals. *Phys. Status Solidi A* **2012**, *209*, 1844–1846.
54. Mimura, A.; Fujii, M.; Hayashi, S.; Kovalev, D.; Koch, F. Photoluminescence and Free-Electron Absorption in Heavily Phosphorus-Doped Si Nanocrystals. *Phys. Rev. B: Condens. Matter Mater. Phys.* **2000**, *62*, 12625.
55. Fujii, M.; Mimura, A.; Hayashi, S.; Yamamoto, Y.; Murakami, K. Hyperfine Structure of the Electron Spin Resonance of Phosphorus-Doped Si Nanocrystals. *Phys. Rev. Lett.* **2002**, *89*, 206805.
56. Sato, K.; Niino, K.; Fukata, N.; Hirakuri, K.; Yamauchi, Y. The Synthesis and Structural Characterization of Boron-Doped Silicon Nanocrystals with Enhanced Electroconductivity. *Nanotechnology* **2009**, *20*, 365207.
57. Hao, X. J.; Cho, E.-C.; Flynn, C.; Shen, Y. S.; Conibeer, G.; Green, M. A. Effects of Boron Doping on the Structural and Optical Properties of Silicon Nanocrystals in a Silicon Dioxide Matrix. *Nanotechnology* **2008**, *19*, 424019.
58. Pi, X.; Chen, X.; Ma, Y.; Yang, D. Optical Absorption and Emission of Nitrogen-Doped Silicon Nanocrystals. *Nanoscale* **2011**, *3*, 4584–4588.
59. Pi, X. Doping Silicon Nanocrystals with Boron and Phosphorus. *J. Nanomater.* **2012**, *2012*, 912903.
60. Ma, Y.; Chen, X.; Pi, X.; Yang, D. Lightly Boron and Phosphorus Co-doped Silicon Nanocrystals. *J. Nanopart. Res.* **2012**, *14*, 802.
61. Lechner, R.; Stegner, A. R.; Pereira, R. N.; Dietmueller, R.; Brandt, M. S.; Ebbers, A.; Trocha, M.; Wiggers, H.; Stutzmann, M. Electronic Properties of Doped Silicon Nanocrystal Films. *J. Appl. Phys.* **2008**, *104*, 053701.
62. Nie, H.; Li, M.; Li, Q.; Liang, S.; Tan, Y.; Sheng, L.; Shi, W.; Zhang, S. X. Carbon Dots with Continuously Tunable Full-Color Emission and Their Application in Ratiometric pH Sensing. *Chem. Mater.* **2014**, *26*, 3104–3112.
63. Belyakov, V. A.; Burdov, V. A.; Lockwood, R.; Meldrum, A. Silicon Nanocrystals: Fundamental Theory and Implications for Stimulated Emission. *Adv. Opt. Technol.* **2008**, *2008*, 279502.
64. Woods, M.; Carlsson, S.; Hong, Q.; Patole, S. N.; Lie, L. H.; Houlton, A.; Horrocks, B. R. A Kinetic Model of the Formation of Organic Monolayers on Hydrogen-Terminated Silicon by Hydrosilation of Alkenes. *J. Phys. Chem. B* **2005**, *109*, 24035–24045.
65. Wolkin, M. V.; Jorne, J.; Fauchet, P. M.; Allan, G.; Delerue, C. Electronic States and Luminescence in Porous Silicon Quantum Dots: The Role of Oxygen. *Phys. Rev. Lett.* **1999**, *82*, 197–200.
66. Marsi, K. L. Phenylsilane Reduction of Phosphine Oxides with Complete Stereospecificity. *J. Org. Chem.* **1974**, *39*, 265–267.
67. Li, Y.; Lu, L.-Q.; Das, S.; Pisiewicz, S.; Junge, K.; Beller, M. Highly Chemoselective Metal-Free Reduction of Phosphine Oxides to Phosphines. *J. Am. Chem. Soc.* **2012**, *134*, 18325–18329.
68. Riduan, S. N.; Zhang, Y.; Ying, J. Y. Conversion of Carbon Dioxide Into Methanol with Silanes Over N-Heterocyclic Carbene Catalyst. *Angew. Chem., Int. Ed.* **2009**, *48*, 3322–3325.
69. Ménard, G.; Stephan, D. W. Room Temperature Reduction of CO_2 to Methanol by Al-Based Frustrated Lewis Pairs and Ammonia Borane. *J. Am. Chem. Soc.* **2010**, *132*, 1796–1797.
70. Green, W. H.; Le, K. P.; Grey, J.; Au, T. T. Sailor, M. J. White Phosphors from a Silicate-Carboxylate Sol-Gel Precursor That Lack Metal Activator Ions. *Science* **1997**, *276*, 1826–1828.
71. Manhat, B. A.; Brown, A. L.; Black, L. A.; Ross, J. B. A.; Fichter, K.; Vu, T.; Richman, E.; Goforth, A. M. One-Step Melt Synthesis of Water-Soluble, Photoluminescent, Surface-Oxidized Silicon Nanoparticles for Cellular Imaging Applications. *Chem. Mater.* **2011**, *23*, 2407–2418.
72. Li, Y.; Chen, C.; Li, J. T.; Yang, Y.; Lin, Z. M. Surface Charges and Optical Characteristic of Colloidal Cubic SiC Nanocrystals. *Nanoscale Res. Lett.* **2011**, *6*, 454.
73. Fan, J.; Li, H.; Jiang, J.; So, L. K. Y.; Lam, Y. W.; Chu, P. K. 3C−SiC Nanocrystals as Fluorescent Biological Labels. *Small* **2008**, *4*, 1058–1062.
74. Bashouti, M. Y.; Sardashti, K.; Schmitt, S. W.; Pietsch, M.; Ristein, J.; Haick, H.; Christiansen, S. H. Oxide-Free Hybrid Silicon Nanowires: From Fundamentals to Applied Nanotechnology. *Prog. Surf. Sci.* **2013**, *88*, 39–60.
75. Li, Q.; He, Y.; Chang, J.; Wang, L.; Chen, H.; Tan, Y.-W.; Wang, H.; Shao, Z. Surface-Modified Silicon Nanoparticles with Ultrabright Photoluminescence and Single-Exponential Decay for Nanoscale Fluorescence Lifetime Imaging of Temperature. *J. Am. Chem. Soc.* **2013**, *135*, 14924–14927.
76. Williams, A. T. R.; Winfield, S. A.; Miller, J. N. Relative Fluorescence Quantum Yields Using a Computer Controlled Luminescence Spectrometer. *Analyst* **1983**, *108*, 1067–1071.